

# Bioorthogonal PEGylation Prolongs the Elimination Half-Life of N-TIMP2 While Retaining MMP Inhibition

Hezi Hayun, Valeria Arkadash, Amiram Sananes, Eyal Arbely, David Stepensky, and Niv Papo\*



Cite This: <https://doi.org/10.1021/acs.bioconjchem.2c00059>



Read Online

ACCESS |



Metrics & More



Article Recommendations

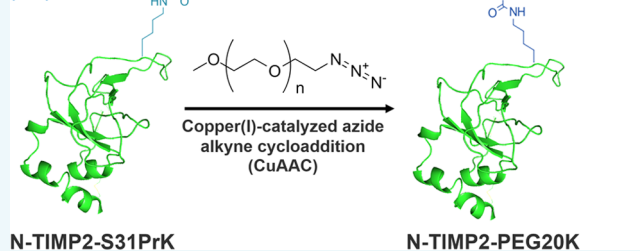


Supporting Information

**ABSTRACT:** Tissue inhibitors of metalloproteinases (TIMPs) are natural inhibitors of the matrix metalloproteinase (MMP) family of proteins, whose members are key regulators of the proteolysis of extracellular matrix components and hence of multiple biological processes. In particular, imbalanced activity of matrix metalloproteinase-14 (MMP-14) may lead to the development of cancer and cardiovascular and other diseases. This study aimed to engineer TIMP2, one of the four homologous TIMPs, as a potential therapeutic by virtue of its ability to bind to the active-site  $Zn^{2+}$  of MMP-14. However, the susceptibility to degradation of TIMP2 and its small size, which results in a short circulation half-life, limit its use as a therapeutic. PEGylation was thus used to improve the pharmacokinetic profile of TIMP2. PEGylation of the MMP-targeting N-terminal domain of TIMP2 (N-TIMP2), via either cysteine or lysine residues, resulted in a significant decrease in N-TIMP2 affinity toward MMP-14 or multisite conjugation and conjugate heterogeneity, respectively. Our strategy designed to address this problem was based on incorporating a noncanonical amino acid (NCAA) into N-TIMP2 to enable site-specific mono-PEGylation. The first step was to incorporate the NCAA propargyl lysine (PrK) at position S31 in N-TIMP2, which does not interfere with the N-TIMP2–MMP-14 binding interface. Thereafter, site-specific PEGylation was achieved via a click chemistry reaction between N-TIMP2-S31PrK and PEG-azide-20K. Inhibition studies showed that PEGylated N-TIMP2-S31PrK did indeed retain its inhibitory activity toward MMP-14. The modified protein also showed improved serum stability vs non-PEGylated N-TIMP2. In vivo pharmacokinetic studies in mice revealed a significant 8-fold increase in the elimination half-life of PEGylated N-TIMP2 vs the non-PEGylated protein. This study shows that site-specific bioorthogonal mono-PEGylation extends the half-life of N-TIMP2 without impairing its biological activity, thereby highlighting the advantage of this strategy for generating potent PEGylated proteins.

## Site-specific PEGylation of N-TIMP2

Genetically encoded propargyl lysine (PrK)



N-TIMP2-S31PrK

N-TIMP2-PEG20K

## INTRODUCTION

Human matrix metalloproteinases (MMPs) comprise a family of 28 known zinc-dependent catalytic enzymes that play major roles in the degradation of extracellular matrix (ECM) components. By virtue of these roles in ECM remodeling, MMPs are significant determinants in multiple biological processes, such as cancer development, angiogenesis, wound healing, tissue repair, and embryogenesis.<sup>1</sup> Any imbalance in the expression and catalytic activity of the different MMPs may thus promote pathological conditions, including arthritis, cardiovascular diseases, and cancer progression, invasion, and metastasis.<sup>1–4</sup> MMPs are therefore considered to be important therapeutic targets, and continuous efforts are underway to develop high-affinity inhibitors with good specificity for particular MMPs.

Selective targeting of MMPs is especially important in the development of therapeutics for cancer-related processes, since the various MMPs play different roles in the promotion of tumor cell migration, proliferation, ECM remodeling, angiogenesis, invasion and metastasis through the cleavage and

activation of multiple proteins.<sup>4–7</sup> A number of studies have shown that expression of MMP-14 (also known as membrane-type-1 MMP or MT1-MMP) is elevated in various human carcinomas, including lung,<sup>8</sup> breast,<sup>9</sup> colon,<sup>10</sup> liver,<sup>11</sup> head and neck,<sup>12</sup> skin,<sup>13,14</sup> and ovarian<sup>15</sup> cancers. Other studies have shown that elevated MMP-14 expression is associated with the early death of patients with various carcinomas, including breast cancer,<sup>12</sup> and is also correlated with lymph node metastasis, tumor invasion, a poor clinical stage, larger tumor size, and progressing tumor stage.<sup>9</sup> Similar observations have also been documented for MMP-2 under various physiological and pathological conditions.<sup>16–18</sup>

Received: February 2, 2022

Revised: April 5, 2022

Because of the obvious importance of MMPs in cancer-related processes, many MMP inhibitors have been designed over the past 40 years. Yet, to date, all of them have failed in clinical trials, probably due to their high toxicity,<sup>19,20</sup> their nonspecific metal binding (i.e., binding not only to zinc but also to the metals in metalloproteins other than MMPs), and poor solubility.<sup>21</sup> Antibodies that have been raised against MMP-2/MMP-9<sup>22</sup> and against MMP-14<sup>23</sup> have shown therapeutic promise in preclinical models, but their development as therapeutics has been impeded by the well-known limitations associated with antibodies, including the high cost of their recombinant production in mammalian cells,<sup>24</sup> their lack of amenability to site-specific incorporation of chemical modalities, and their potential undesired effector functions,<sup>25</sup> together with considerable intellectual property barriers to their development.<sup>26</sup>

Attractive alternatives to antibodies are the four members of the mammalian tissue inhibitor of the metalloproteinases (TIMP) family (TIMP1–4). These homologous TIMPs inhibit MMP activity by the same mechanism, namely, the conserved TIMP Cys1 residue coordinates the catalytic Zn<sup>2+</sup> ion of the MMP, thereby preventing the substrate cleavage process.<sup>27</sup> The four TIMP members show 40–50% sequence identity to each other and exhibit slightly different preferences for various MMPs.<sup>28</sup> In particular, TIMP2 shows promise as a natural broad inhibitor of the MMP family in that it exhibits high affinity toward various MMPs (10<sup>-10</sup>–10<sup>-9</sup> M), while being nontoxic to humans and nonimmunogenic. Support for the notion of using TIMP2 as an MMP inhibitor may be drawn from a study showing that TIMP2 possesses a dual regulatory function toward MMP-14 and its natural substrate MMP-2,<sup>29</sup> i.e., TIMP2 simultaneously binds to the catalytic site of MMP-14, via its N-terminal domain (N-TIMP2), and to the hemopexin domain of proMMP-2, via its C-terminal domain (C-TIMP2). The ternary complex (MMP-14-TIMP2-proMMP-2) so formed carries proMMP-2 to the cell membrane, where it becomes accessible for activation by free MMP-14.<sup>5,30,31</sup> Of note, when the C-terminal domain of TIMP2 is absent, the N-TIMP2 fragment (residues 1–127) neither binds nor activates proMMP-2, although it retains its full MMP (both MMP-14 and MMP-2) inhibitory activity.<sup>32,33</sup>

Despite the promise of TIMPs as potential inhibitors of MMPs, their development for therapeutic purposes is hampered by the major limitation of their short circulation half-life, due to their small size. For example, it was shown that murine TIMP1 (24.5 kDa) injected into rats was cleared from the plasma within minutes.<sup>34</sup> Similarly, the distribution half-life and the elimination half-life of recombinant human TIMP1 were reported to be low in mice, namely, 0.22–1 h and 1–4 h, respectively.<sup>35,36</sup> In a clinical study, N-TIMP2 (15 kDa) injected into patients with Kaposi sarcoma was rapidly cleared from the blood, with a short first-component half-time of approximately 17 min and a second component half-time of approximately 10 h, and therefore did not accumulate efficiently in the tumors.<sup>37</sup> These findings suggest that TIMPs cannot be used as such for therapeutic purposes.

We, therefore, sought to exploit a strategy commonly used for enhancing the circulation half-life of proteins, namely, increasing their size by PEGylation. However, the common approaches for protein PEGylation, i.e., the conjugation of poly(ethylene glycol) (PEG) molecules to the side chains of cysteine via a maleimide labeling chemistry or lysine via *N*-hydroxysuccinimide (NHS) ester chemical cross-linking, quite

often lead to undesired random and multisite conjugation (unless complicated multistep techniques for activating or protecting specific residues are used). The resulting side products may affect the protein stability and functionality and may complicate processes of purification, characterization, and function analysis.<sup>38–40</sup>

One possible solution to this type of problem is to use genetic code expansion technology to site-specifically incorporate a noncanonical amino acid (NCAA) into the target protein. The NCAA can carry a chemical handle for downstream bioorthogonal conjugation, thereby providing a way to overcome the limitations of random and multisite conjugations and hence to produce proteins with improved pharmacokinetic properties.<sup>41–44</sup> Cotranslational incorporation of the NCAA in response to a unique codon (usually the UAG stop codon) is achieved by using an orthogonal aminoacyl-tRNA synthetase (aaRS)/tRNA pair, e.g., the pyrrolysine tRNA synthetase/tRNA pair obtained from methanogenic archaea (PylRS/PylT pair).<sup>45,46</sup> Incorporation of NCAs that possess particular functional groups has been used for site-specific protein conjugation for a variety of applications, such as labeling, imaging, antibody–drug conjugation, and site-selective PEGylation.<sup>38,47–49</sup> The last of these approaches has already been applied to overcome the limitations of protein multisite PEGylation via canonical amino acids (i.e., Lys or Cys),<sup>43,50</sup> and this technique has recently been implemented for therapeutic<sup>51</sup> and imaging<sup>52,53</sup> applications.

In the current study, we generated an alkyne-bearing N-TIMP2 via the incorporation of the NCAA propargyl lysine (PrK) at position 31 (a position that is not involved in MMP binding<sup>54</sup> and is hence tolerant to mutagenesis). The PrK-bearing N-TIMP2 was then site-specifically conjugated to mPEG-azide-20K (methoxy PEG azide with a molecular weight of 20 kDa) via a Cu(I)-catalyzed click reaction. This site-specific and mono-PEGylated N-TIMP2 (i.e., N-TIMP2 labeled with PEG at a single position) exhibited significantly higher affinity toward MMP-14 than N-TIMP2 PEGylated via a cysteine residue. In addition, relative to non-PEGylated N-TIMP2, mono-PEGylated N-TIMP2 retained its affinity and its inhibitory potency toward MMP-14 but exhibited higher resistance to serum proteases. Notably, the mono-PEGylated N-TIMP2 exhibited an 8-fold improvement in the circulation half-life (25.8 h for PEGylated N-TIMP2 vs 3.11 h for non-PEGylated N-TIMP2). This work thus demonstrates the advantage of utilizing a genetically encoded bioorthogonal chemical handle for the production of homogeneously and site-specifically PEGylated proteins as a means to improve the circulation half-life of proteins without impairing their biological activity.

## RESULTS AND DISCUSSION

**PEGylation of N-TIMP2 via Cysteine and Lysine Residues.** To produce PEGylated N-TIMP2 via a cysteine residue, we took as the starting material, a variant of N-TIMP2, designated N-TIMP2<sub>D</sub>, which is a highly potent inhibitor of MMP-14 that we had previously prepared in our laboratory.<sup>55</sup> To conjugate N-TIMP2<sub>D</sub> to PEG by a maleimide reaction on a cysteine residue, we first prepared the compound designated N-TIMP2<sub>D-Cys</sub> by introducing a free cysteine residue into N-TIMP2<sub>D</sub> (at the C-terminus) through the addition of a flexible linker having five repeats of the GGGGS sequence followed by a cysteine residue. We purified N-TIMP2<sub>D-Cys</sub> by affinity and

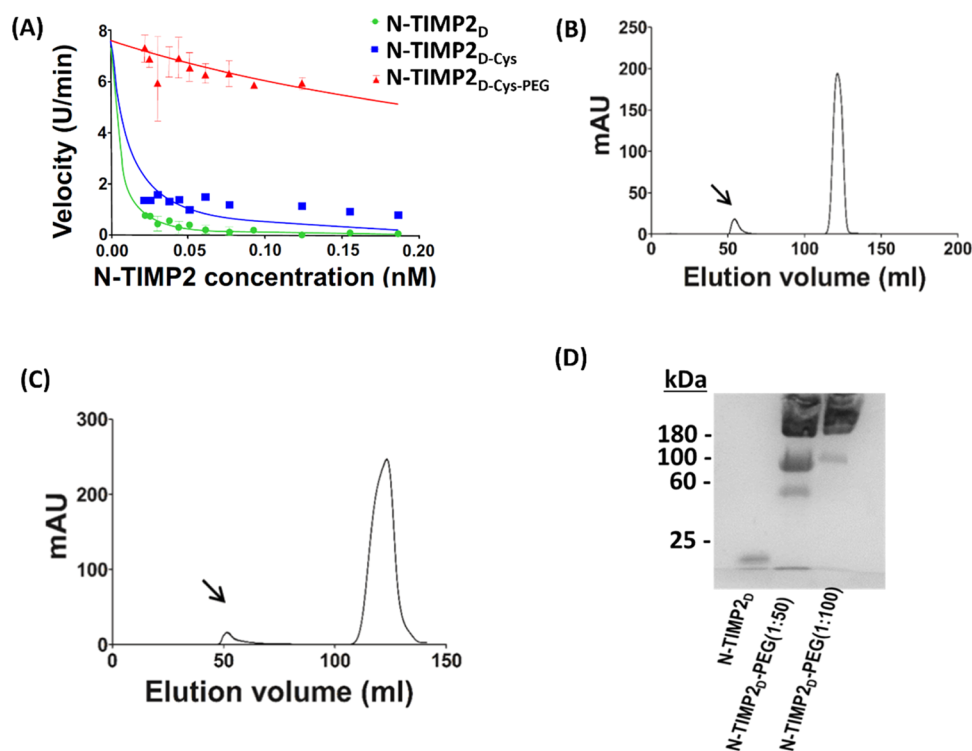


**Figure 1.** PEGylation of N-TIMP2 via canonical amino acids: PEGylation of N-TIMP2<sub>D</sub> via C-terminal cysteine residues with mPEG-30K (A) and via lysine residues with mPEG-SCM-20K (B–D). (A) MMP-14<sub>CAT</sub> inhibition by various concentrations of N-TIMP2<sub>D</sub>, N-TIMP2<sub>D-Cys</sub>, and N-TIMP2<sub>D-Cys-PEG</sub>. Cleavage of the fluorescent substrate was measured over time, and the velocity (slope) of the reaction as a function of inhibitor concentration was fitted by Morrison's equation (eq 1) to obtain the inhibition constant  $K_i$ . (B and C) SEC analysis of N-TIMP2<sub>D</sub> conjugated with a 50 or 100 molar excess of PEG20K, respectively. The peaks marked with arrows were collected for further analysis. (D) 10% SDS-PAGE analysis of N-TIMP2<sub>D</sub>-PEG fractions under reducing conditions.

size-exclusion chromatography (SEC) and confirmed its purity and size by sodium dodecyl sulfate–polyacrylamide gel electrophoresis (SDS-PAGE) and mass spectrometry. For the PEGylation reaction, N-TIMP2<sub>D-Cys</sub> was treated with a reducing agent before incubating it with an excess of mPEG-30K. SEC was then used to separate the PEGylated material from the unconjugated protein. Lastly, the inhibitory activities of N-TIMP2<sub>D</sub> vs N-TIMP2<sub>D-Cys</sub> and N-TIMP2<sub>D-Cys-PEG</sub> were examined in an enzymatic assay. For that purpose, the catalytic domain of MMP-14 (designated MMP-14<sub>CAT</sub>) was incubated with increasing concentrations of N-TIMP2<sub>D</sub>, N-TIMP2<sub>D-Cys</sub>, and N-TIMP2<sub>D-Cys-PEG</sub>, and the cleavage of a fluorogenic substrate was determined as a function of time. To determine the inhibition constants ( $K_i$ ) (Figure 1A), the slope of each catalytic reaction was calculated and fitted to Morrison's tight-binding equation (eq 1; see Methods). The  $K_i$  values obtained in the assay showed no significant difference between the inhibitory potencies of N-TIMP2<sub>D</sub> ( $0.004 \pm 0.001$  nM) and N-TIMP2<sub>D-Cys</sub> ( $0.008 \pm 0.002$  nM) toward MMP-14, indicating that the addition of the Cys residue to the C-terminus of N-TIMP2 did not disrupt protein function. In contrast, the  $K_i$  value obtained for N-TIMP2<sub>D-Cys-PEG</sub> was  $0.18 \pm 0.03$  nM, which was a significant (45-fold) decrease in the affinity to MMP-14, compared to N-TIMP2<sub>D</sub>, indicating a loss of function upon PEGylation.

The explanation for the above loss of function for the PEGylated N-TIMP2<sub>D-Cys-PEG</sub> compound may be derived from its mode of preparation, in that conjugation of PEG to a free thiol by a maleimide reaction requires preincubation of the protein with a reducing agent. It is possible that the reducing

agent disrupted the three native intramolecular disulfide bonds (formed by six Cys residues) of N-TIMP2, leading to the formation of non-native intra- or intermolecular bonds and hence to non-functional structures of the protein. Another possible explanation could be the undesired modification of the free N-terminus of N-TIMP2 due to conjugation to PEG via the Cys residues (i.e., Cys1 and/or Cys3) that are essential for the MMP inhibitory activity of N-TIMP2. These alterations—whether in the conformation of the protein, in its oligomerization state, or in its N-terminus (i.e., interface with the MMP target molecule)—may be the reason for the observed significant decrease in the inhibitory activity of N-TIMP2<sub>D-Cys-PEG</sub> toward MMP-14 and indicate that this approach is unsuitable for PEGylation of N-TIMP2. These results are in agreement with the findings of the study of Batra et al.,<sup>36</sup> in which the conjugation of PEG to full-length human TIMP1 was performed via the incorporation of a Cys residue at positions 180, 181, 182, or 183 within the protein. The reaction took place only in the presence of a weak reducing agent that facilitated partial reduction and deprotection of the individual incorporated Cys residue, without disrupting the native disulfide bonds (generated by the other cysteines) in TIMP1. However, this site-specific PEGylation severely affected TIMP1 inhibitory activity toward MMP-3.

Our second approach for N-TIMP2<sub>D</sub> PEGylation was to conjugate PEG to the lysine residues of N-TIMP2. To this end, N-TIMP2<sub>D</sub> was incubated with mPEG-SCM-20K at two different molar ratios (1:50 and 1:100 protein:mPEG-SCM-20K). Thereafter, SEC was applied to separate the PEGylated product from the unconjugated protein (Figure 1B,C), and the

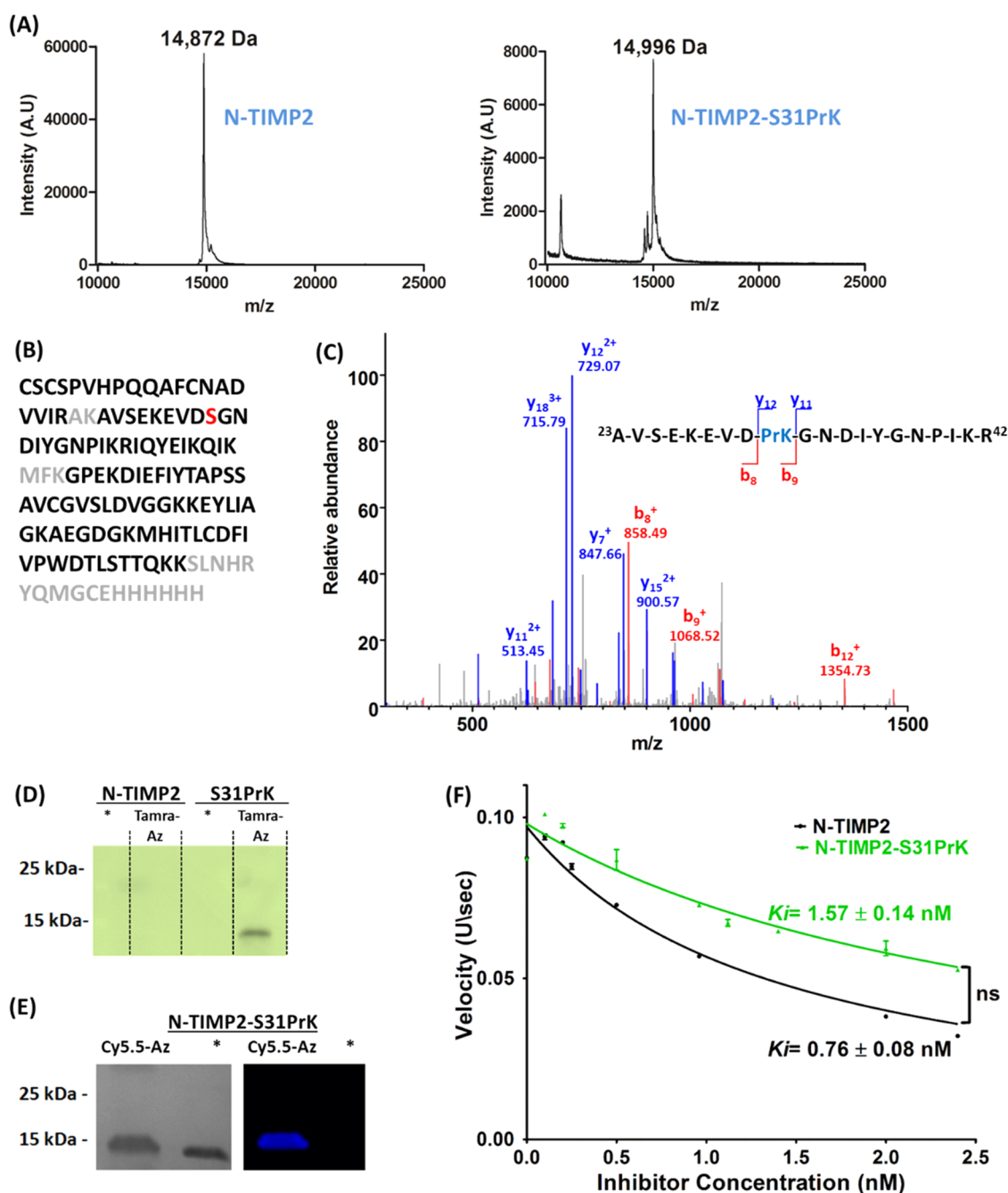


**Figure 2.** Incorporation of PrK into N-TIMP2-S31TAG. (A) Mass spectrometry analysis of N-TIMP2 (left, expected mass: 14,883 Da) and N-TIMP2-S31PrK (right, expected mass: 15,006 Da) confirming the correct mass difference of ~123 Da between the proteins. Differences between expected (theoretical) and observed values were less than 0.1%. (B) Illustration of the sequence coverage of N-TIMP2-S31PrK by liquid chromatography-tandem mass spectrometry (LC-MS)/MS analysis following trypsin digestion. Sequence coverage was determined as 83.46% with a 100% sequence match (black—identified amino acids; red—incorporation site of PrK; gray—not identified). (C) LC-MS/MS analysis confirming the incorporation of PrK at position 31. (D) Fluorescence SDS-PAGE analysis of N-TIMP2 or N-TIMP2-S31PrK upon a click reaction with TAMRA-azide. (E) Coomassie-stained (left) and fluorescence (right) SDS-PAGE analysis of purified N-TIMP2-S31PrK and the Cy5.5-azide reaction product. Asterisks indicate samples that did not undergo a click reaction. (F) MMP-14 inhibitory activity of N-TIMP2 and N-TIMP2-S31PrK. MMP-14<sub>CAT</sub> was incubated with various concentrations of N-TIMP2 and N-TIMP2-S31PrK (0–2.4 nM). The substrate degradation velocity was fitted to Morrison's equation (eq 1; see Methods) to obtain  $K_i$  values. Error bars represent the standard error of the mean (SEM);  $n = 3$ . ns, not significant by the  $t$ -test comparison of N-TIMP2 and N-TIMP2-S31PrK.

eluted fractions were resolved by SDS-PAGE (Figure 1D). Several bands for each of the two samples were detected in the gels, indicating conjugation of one or more PEG molecules to N-TIMP2<sub>D</sub>. However, we did not follow up with these fractions for further study due to the unsuccessful separation (by SEC) of the heterogeneous mixtures that resulted from the

multisite, random PEG conjugation to N-TIMP2<sub>D</sub>, which has 11 lysine residues. Similar nonspecific PEGylation was also demonstrated for TIMP1 in which lysine residues were conjugated to mPEG-5K or mPEG-20K, resulting in product mixtures of TIMP1 conjugated to either 4–7 mPEG-SCM-5K or 1–2 mPEG-SCM-20K molecules.<sup>36</sup> Studies with other

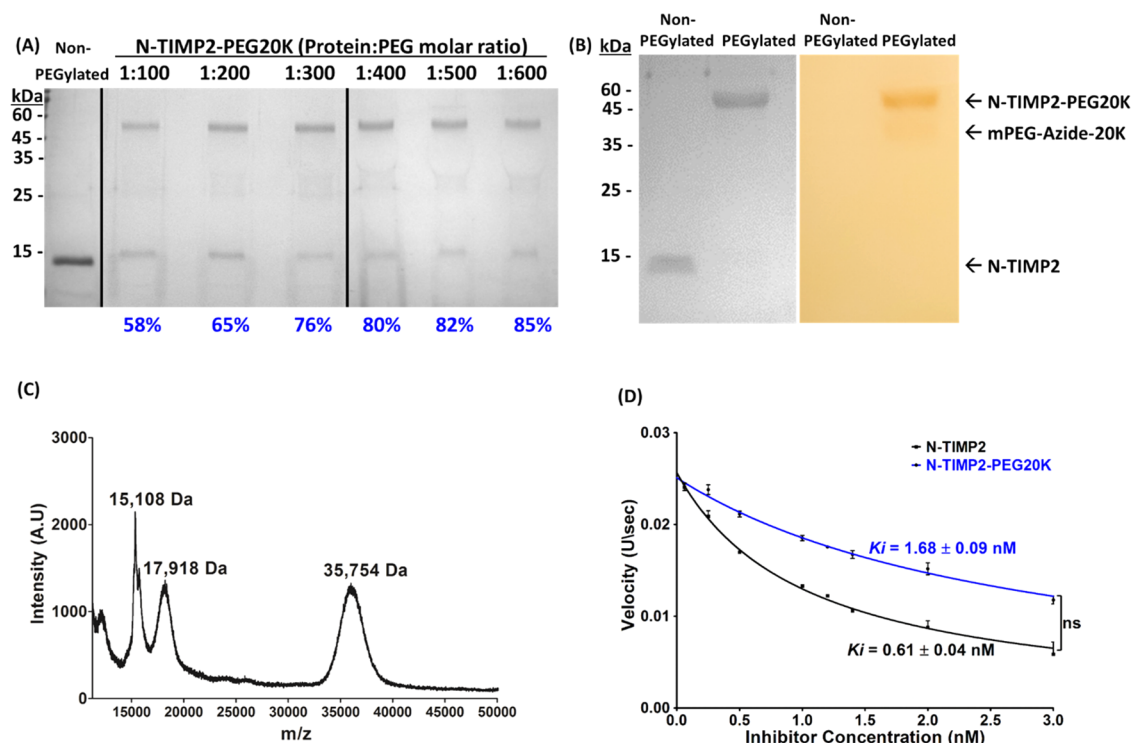


**Figure 3.** Site-specific PEGylation of N-TIMP2 via a click reaction. (A) SDS-PAGE analysis of N-TIMP2-S31PrK PEGylation with different protein:mPEG-azide-20K ratios. Samples were ran on 15% polyacrylamide gel under reducing conditions. Labeling yields (values in blue) were calculated using ImageJ. (B) SDS-PAGE analysis of purified non-PEGylated and PEGylated N-TIMP2 by Coomassie staining for protein visualization (left) and barium iodide staining for PEG visualization (right). The left lanes in panels (A) and (B) show non-PEGylated N-TIMP2-S31PrK. (C) MALDI-TOF mass spectrometry analysis of N-TIMP2-PEG20K. The spectrum shows peaks centered at 35,724 Da ( $z = 1$ ) and at 17,918 Da ( $z = 2$ ), indicating mono-PEGylation of N-TIMP2 with PEG20K, and a peak for the non-PEGylated protein (15,107 Da), indicating that some non-PEGylated protein had not been removed in the purification step. (D) Substrate degradation velocities of N-TIMP2 and N-TIMP2-PEG20K (0–3 nM) by MMP-14<sub>CAT</sub>. The substrate degradation velocity was fitted to Morrison's equation (eq 1) to obtain  $K_i$  values. Error bars represent SEM;  $n = 3$ . ns, not significant by a  $t$ -test.

proteins reported similar limitations for PEGylation, such as the generation of a heterogeneous mixture and decreased activity (7–28%) for PEGylated interferon- $\alpha 2$ ,<sup>56</sup> decreased activity (20- to 30-fold) upon site-directed PEGylation of trichosanthin,<sup>57</sup> and decreased antigen binding (17 and 62%) for multisite PEGylated Fab.<sup>40</sup>

**N-TIMP2 Mutagenesis for Site-Specific PrK Incorporation.** To overcome the above limitations of the formation of a heterogeneous product and/or reduced potency (as shown in Figure 1A), we chose to perform site-specific PEGylation of N-TIMP2 by genetically encoding the incorporation of a single propargyl lysine residue (PrK, Figure S1A) into N-TIMP2 at a selected position (position S31). The NCAA PrK possesses an alkyne group that can be utilized for bioorthogonal conjugation to the PEG-azide molecule via a classic azide–alkyne click reaction. To maintain the stability and functionality of N-TIMP2, two main considerations influenced our choice of the N-TIMP2 PEGylation site: (1) modification of the position should cause minimal disruption to the protein structure (e.g., formation of disulfide bonds or secondary structures) or minimal disruption to the interaction of N-TIMP2 (at its N-terminus or at other binding loops, i.e., positions 35–42, 66–72, 97–99<sup>55</sup>) with MMP-14 (Figure S1B)<sup>58</sup> and (2) the position should be solvent-exposed to allow facile and efficient conjugation of PEG to N-TIMP2. Therefore, we decided to incorporate PrK into position S31, which is located on an exposed loop of N-TIMP2 (Figure S1B) and meets all of the requirements mentioned above. To this end, we introduced an

in-frame stop codon (TAG) mutation at position S31 and used the PylRS/PylT pair from *Methanosarcina mazei* to direct the cotranslational incorporation of PrK in response to the TAG codon.

**Validation and Characterization of PrK Incorporation into N-TIMP2-S31TAG.** To express N-TIMP2-S31PrK, we cotransformed the *Escherichia coli* strain WK6 with two plasmids, namely, (i) pMECS, containing the N-TIMP2-S31TAG gene for expression of N-TIMP2 with a C-terminal 6×His tag and (ii) pEVOL-MmPyl, containing the genes for the orthogonal PylRS/PylT pair. Western blot analysis using an antibody against the C-terminal 6×His tag showed that expression of full-length N-TIMP2-S31PrK (~15 kDa) was NCAA dependent, as expected (Figure S2). Minor expression of full-length N-TIMP2-S31PrK was observed in the absence of the NCAA, since the pEVOL plasmid has two copies of the *M. mazei* PylRS gene, under the control of either constitutive or arabinose-inducible promoters.<sup>59</sup>

Wild-type N-TIMP2 (Figure S3) and N-TIMP2-S31PrK were expressed in WK6 bacteria and purified by Ni<sup>2+</sup> affinity chromatography. Mass spectrometry confirmed the incorporation of a single PrK residue into N-TIMP2-S31TAG. Specifically, matrix-assisted laser desorption/ionization-time-of-flight (MALDI-TOF) analysis gave the expected mass difference of ~123.15 Da between N-TIMP2 and N-TIMP2-S31PrK (Figure 2A). Of note, two additional small peaks were also observed in the mass spectrum. However, the mass differences of –411 and –275 Da relative to the molecular

weight of N-TIMP2-S31PrK (observed for the small peaks in Figure 2A) are not in agreement with either misincorporation of a canonical amino acid or the molecular weight of native N-TIMP2. In fact, the fidelity of the wild-type pyrrolysine tRNA synthetase is well documented, and therefore we expect minimal misincorporation when TAG-mutant proteins are expressed in the presence of an NCAA. Therefore, these additional peaks are probably due to impurities or a truncated version of the expressed protein. Since the His tag (used to purify the protein) is located at the C-terminus, these anomalies could be attributed to N-truncated proteins.

To confirm the site-specific incorporation of PrK, N-TIMP2-S31PrK was then analyzed by LC-MS/MS following trypsin digestion, resulting in a sequence coverage of 83.46% (Figure 2B), including the PrK incorporation site. As expected, the MS/MS spectrum of the peptide fragment<sup>23</sup>A-R<sup>42</sup> confirmed the successful incorporation of PrK at position 31 (Figure 2C). To investigate the feasibility of PEGylating N-TIMP2-S31PrK by click chemistry, we first performed a click reaction using two different azide-conjugated fluorophores, i.e., tetramethylrhodamine-azide (Tamra-Az) and Cyanine5.5 azide (Cy5.5-Az), followed by in-gel fluorescence analysis of the conjugated product (Figure 2D,E). Our results indicated efficient conjugation of the azide moieties and N-TIMP2-S31PrK; as expected, no conjugation was observed for N-TIMP2, which lacks an alkyne group, as was also shown for other proteins.<sup>60,61</sup> To ensure that N-TIMP2-S31PrK was correctly folded and fully functional (i.e., has the same inhibition of MMP-14 activity as the parental N-TIMP2), an MMP-14 activity assay was performed (Figure 2F). The observed  $K_i$  values were  $0.76 \pm 0.08$  and  $1.57 \pm 0.17$  nM for N-TIMP2 and N-TIMP2-S31PrK, respectively, with both values being consistent with previously reported  $K_i$  values for N-TIMP2 inhibition of MMP-14.<sup>55,62</sup> The finding that there was no significant difference between the inhibitory potencies of N-TIMP2-S31PrK and N-TIMP2 confirmed that the incorporation of PrK into position 31 of N-TIMP2 had not impaired its folding or its inhibitory activity toward MMP-14. These results thus confirmed the tolerance of position 31 in N-TIMP2 to mutagenesis in terms of the maintenance of potency.

**Site-Specific Mono-PEGylation of N-TIMP2.** To determine the optimal conditions for PrK-mediated PEGylation of N-TIMP2-S31PrK with mPEG-azide-20K, we tested reaction mixtures having different protein:PEG20K molar ratios (1:100 to 1:600, Figure 3A). We found that a molar ratio of 1:400 resulted in an 80% conjugation yield, and a higher PEG excess did not markedly improve PEG conjugation. Large-scale PEGylation was thus performed using a 1:400 protein:PEG molar ratio, and the resulting N-TIMP2-PEG20K product was purified by ion-exchange chromatography. SDS-PAGE analysis of the purified N-TIMP2-PEG20K protein conjugate, which has a theoretical molecular weight of 35 kDa, revealed a ~50 kDa band (Figure 3B, left). The ~15 kDa difference in molecular weights can be explained in terms of the negatively charged complex formed between PEG molecules and SDS micelles, causing the PEGylated proteins to migrate more slowly on the gel.<sup>63</sup> A similar disparity of ~15 kDa has been found upon SDS-PAGE for other proteins conjugated to PEG20K, e.g., human serum albumin<sup>63</sup> and TIMP1.<sup>36</sup> In the current study, the conjugation of PEG was confirmed by barium iodide staining (Figure 3B, right). In addition, purified N-TIMP2-PEG20K was analyzed by MALDI-TOF mass

spectrometry, which confirmed the mono-PEGylation of N-TIMP2, with a peak centered at ~35 kDa, as expected (Figure 3C). The generation of a mono-PEGylated protein via a click reaction is in line with other studies in which protein PEGylation via Cu<sup>I</sup>-catalyzed click chemistry was accomplished using genetically encoded azide- or alkyne-containing NCAs.<sup>43,50</sup>

Purified N-TIMP2-PEG20K was then evaluated for its potency in inhibiting MMP-14. An in vitro activity assay showed that N-TIMP2-PEG20K retained its inhibitory activity toward MMP-14<sub>CAT</sub>, with a  $K_i$  of  $1.68 \pm 0.09$  nM (Figure 3D). These findings suggest that our approach for site-specific PEGylation of N-TIMP2 was successful in producing a mono-PEGylated product that retained its inhibitory potency toward MMP-14. This maintenance of inhibitory potency is especially important in light of the decreased activity that was observed in this work for N-TIMP2<sub>D-Cys</sub>-PEG and for other therapeutic PEGylated proteins.<sup>36,40,56,57</sup>

**PEGylation Increases N-TIMP2 Serum Stability.** To evaluate the beneficial effects conferred by PEGylation on the pharmacokinetic profile of N-TIMP2, we first compared the serum stability of N-TIMP2 to that of N-TIMP2-PEG20K. The non-PEGylated and PEGylated proteins were incubated separately in fresh human serum at 37 °C for 18 days, and samples were withdrawn for analysis from each mixture every 2–4 days and stored at –80 °C until analysis. To determine the protein levels over the 18-day course of the experiment, the stored samples were then analyzed by western blot. While a significant (~40%) degradation of N-TIMP2 was observed after as little as 7 days and almost no intact N-TIMP2 was detected after 14 days, N-TIMP2-PEG20K remained remarkably stable throughout the entire experiment, with high levels of intact proteins being maintained for up to 18 days, thereby indicating a much slower degradation rate in comparison with N-TIMP2 (Figure 4). These results clearly indicate that relative to N-TIMP2, N-TIMP2-PEG20K is more resistant to cleavage by proteases (48.4 and 3.6% of intact proteins at day 18 for N-TIMP2-PEG20K and N-TIMP2, respectively), suggesting an improved pharmacokinetic profile for the PEGylated protein. These findings are in agreement with other studies showing PEGylation-enhanced resistance to proteolysis. For example, asparaginase and uricase PEGylated with linear and branched PEG-10K<sup>64</sup> or the WW domain of the human protein Pin 1 PEGylated with 4- or 45-unit PEG oligomers<sup>65</sup> demonstrated higher resistance to cleavage by trypsin, pronase, elastase, or proteinase K compared to the unmodified parental proteins, suggesting that the PEG molecules may shield and protect the protein from enzyme degradation.<sup>66,67</sup>

**PEGylation Prolongs the Elimination Half-Life of N-TIMP2 and Enhances Its Systemic Exposure.** To evaluate the changes in the pharmacokinetic profile of N-TIMP2 due to PEGylation, we carried out an in vivo pharmacokinetic study. Mice were intravenously injected with a bolus of 3 mg/kg N-TIMP2 or N-TIMP2-PEG20K, and the serum levels of the proteins were followed over time for 72 h. Analysis of the time course of N-TIMP2 and N-TIMP2-PEG20K concentrations in the sera revealed a significant 8.3-fold increase (from 3.11 to 25.8 h) in the elimination half-life of N-TIMP2-PEG20K as compared to N-TIMP2 (Figure 5). Importantly, the area under the curve ( $AUC_{0-\infty}$ ) increased 12.2-fold for N-TIMP2-PEG20K (from 69.7  $\mu\text{g}\cdot\text{h}/\text{mL}$  for N-TIMP2 to 851.7  $\mu\text{g}\cdot\text{h}/\text{mL}$  for N-TIMP2-PEG20K). This increase indicates higher

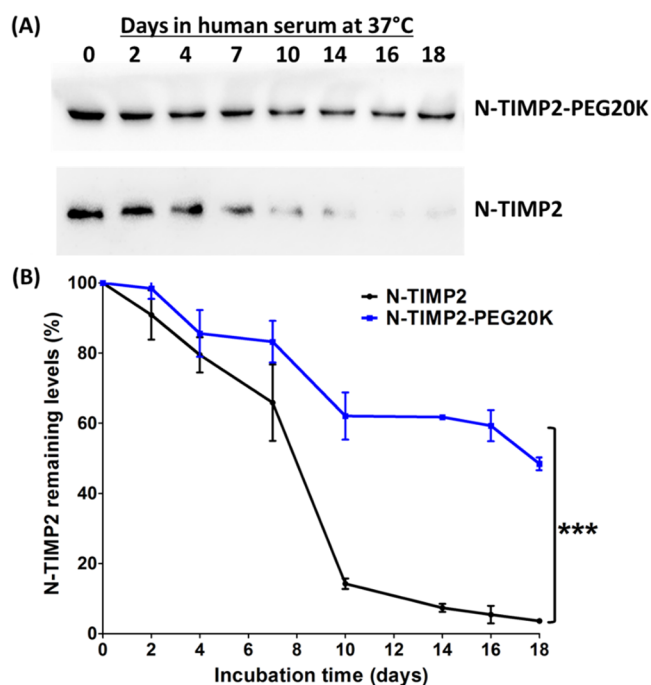


**Figure 4.** PEGylation improves N-TIMP2 stability in human serum. N-TIMP2 and N-TIMP2-PEG20K were incubated in human serum (1:5 v/v) at 37 °C for 18 days, and samples were withdrawn every 2–4 days for analysis. (A) Representative anti-6×His western blot analysis of N-TIMP2 and N-TIMP2-PEG20K samples. (B) Degradation curves normalized to day 0 for each protein. Error bars represent SEM,  $n = 3$ . Statistical analysis for the comparison of N-TIMP2 to N-TIMP2-PEG20K was performed by Student's *t*-test; \*\*\* $P < 0.0001$ .

stability and reduced clearance (vs the non-PEGylated protein) and hence extended systemic exposure to the PEGylated protein, which is expected to enhance its pharmacological activity. An extended circulation half-life due to protein PEGylation has also been shown for a variety of proteins, e.g., interferon- $\alpha 2$  (from 3–8 to 65 h),<sup>56</sup> interleukin-6 (from 2.1 to 206 min),<sup>68</sup> and tumor necrosis factor (from 3 to 45–136 min),<sup>69</sup> all compared to native non-PEGylated proteins.

In conclusion, protein PEGylation serves two purposes. First, by virtue of the large hydrodynamic radius of PEG,<sup>63</sup> PEGylation increases the size of the protein and thereby slows down its clearance from the blood circulation, apparently via reduced glomerular filtration in the kidneys. Second, PEGylation confers resistance to degradation by serum proteases, and hence PEGylated proteins circulate for a longer time, thereby facilitating enhanced systemic exposure, in comparison with non-PEGylated proteins.

## METHODS

**PEGylation of N-TIMP2<sub>D</sub> via Cysteine and Lysine Residues.** N-TIMP2<sub>D</sub>, a highly potent MMP-14 inhibitor generated in our laboratory,<sup>55</sup> was subjected to PEGylation using two different methods, one via cysteine residues and the other via lysine residues. For PEG conjugation via cysteine residues, a free cysteine residue was introduced into N-TIMP2<sub>D</sub> by the addition of a flexible linker comprising five GGGGS repeats followed by a cysteine residue at the C-terminus of N-TIMP2<sub>D</sub>, thereby producing the protein that we designated N-TIMP2<sub>D-Cys</sub>. For PEGylation, N-TIMP2<sub>D-Cys</sub> (400  $\mu$ g) in 50 mM Tris, pH 7.5, 100 mM NaCl, and 5 mM CaCl<sub>2</sub> was incubated with tris(2-carboxyethyl)phosphine (TCEP) (Sigma-Aldrich, Israel) at a 1:1 molar ratio for 20 min at room temperature, followed by washing with a Vivaspin centrifugal concentrator with a 3 kDa cutoff (GE Healthcare Life Sciences, Pittsburgh, PA) and incubation for 1 h at room temperature with mono-methoxypoly(ethylene glycol) (mPEG)-maleimide of molecular weight of 30 kDa (mPEG-30K) (Laysan Bio Inc, Arab, AL) at a 1:20 molar ratio (protein:mPEG). This conjugated protein (designated N-TIMP2<sub>D-Cys-PEG</sub>) was purified in an AKTA pure system (GE Healthcare Life Sciences), equipped with a Superdex 200 column (GE Healthcare Life Sciences), using a buffer comprising 50 mM Tris, pH 7.5, 100 mM NaCl, and 5 mM CaCl<sub>2</sub>. SDS-PAGE analysis of the purification products on a 10% polyacrylamide gel under reducing conditions was then performed, and the bands were visualized by staining with InstantBlue (CBS Scientific, Del Mar, CA). Protein samples were concentrated using a Vivaspin centrifugal concentrator with a 3 kDa cutoff (GE Healthcare Life Sciences). Protein concentrations were determined by UV–vis absorbance at 280

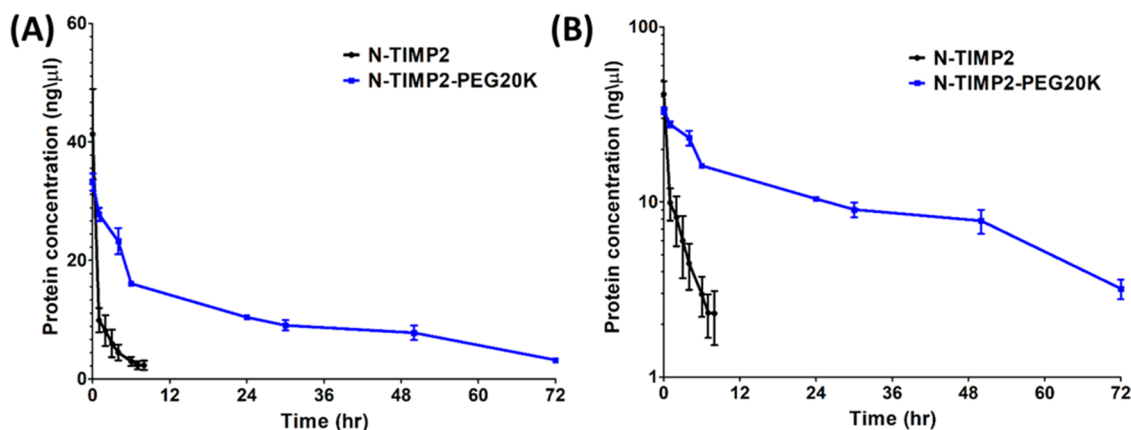


**Figure 5.** PEGylation prolongs the elimination half-life of N-TIMP2 and enhances its systemic exposure. The graphs (A) linear and (B) semilogarithmic show the time course of N-TIMP2 and N-TIMP2-PEG20K serum concentrations after intravenous administration of a 3 mg/kg bolus of N-TIMP2 or N-TIMP2-PEG20K. It may be seen that N-TIMP2 was eliminated rapidly, but the concentrations of N-TIMP2-PEG20K remained high over 72 h. Error bars represent SEM,  $n = 3$ .

nm on a NanoDrop spectrophotometer (Thermo Fisher Scientific), with an extinction coefficient ( $\epsilon_{280}$ ) of 13,500  $M^{-1} \text{ cm}^{-1}$  for all N-TIMP2 variants.

For PEG conjugation via lysine residues, N-TIMP2<sub>D</sub> (1 mg) in phosphate-buffered saline (PBS), pH 7.4, was conjugated to a methoxy PEG-succinimidyl carboxymethyl ester (mPEG-SCM) of molecular weight of 20 kDa (mPEG-SCM-20K) (Jenkem Technology, Allen, TX) at 1:50 and 1:100 molar ratios (protein:mPEG) overnight at 4 °C. Thereafter, the workup for the product conjugated via the lysine residues was the same as that for the product conjugated via the cysteine residues, as described above.

**Generation of N-TIMP2-S31PrK.** To choose the position for the incorporation of PrK into N-TIMP2, the TIMP2-MMP-14 complex (PDB 1BUV) was analyzed in PyMOL (the PyMOL Molecular Graphics System, Version 1.1 Schrödinger, LLC). The gene encoding for N-TIMP2 was cloned into a pMECS expression vector (a kind gift from Dr. Serge Muyldermans, Vrije University of Brussels, Brussels, Belgium) using a restriction-free polymerase chain reaction (RF-PCR),<sup>70</sup> which served as a template for introducing the TAG point mutation in position S31 of N-TIMP2. All plasmid sequences were verified by Sanger sequencing (Genetics Unit, NIBN, Ben-Gurion University of the Negev, Israel). The following primers were used to generate the gene for N-TIMP2-S31TAG:

FWD: 5'-GAAGTGGACTAGGGAAACGACA-3'.

REV: 5'-CTTCTCACTGACCGCTTTGG-3'.

**Production and Purification of N-TIMP2 and N-TIMP2-S31PrK.** The pEVOL vector (a kind gift from Prof. Lital Alfonta, BGU, Beer-Sheva, Israel), containing the *M. maezi* PylRS/tRNA<sub>CUA</sub><sup>pyl</sup> genes for the incorporation of PrK,<sup>71</sup> was cotransformed into the *E. coli* strain WK6 with the pMECS plasmid bearing N-TIMP2-S31TAG. The *E. coli* strain WK6 transformed with the pMECS plasmid containing the wild-type N-TIMP2 gene served as the control. The bacteria were grown at 37 °C in TB medium (17 mM KH<sub>2</sub>PO<sub>4</sub>, 94 mM K<sub>2</sub>HPO<sub>4</sub>, 12 g/L peptone, 24 g/L yeast extract, 0.4% glycerol) containing 100  $\mu\text{g}/\text{mL}$  ampicillin for N-TIMP2 or 100  $\mu\text{g}/\text{mL}$  ampicillin, 50  $\mu\text{g}/\text{mL}$  chloramphenicol, and 1 mM PrK (SynChem, Inc.) for N-TIMP2-S31TAG, with stirring at 200 rpm. At an OD<sub>600</sub> of 0.4, 0.2% arabinose (Mercury, Rosh Ha'ayin, Israel) was added to N-TIMP2-S31TAG (for PylRS induction), and at an OD<sub>600</sub> of 0.6–0.9, the expression of both proteins (N-TIMP2 and N-TIMP2-S31PrK) was induced by addition to the medium of 1 mM IPTG (Sigma-Aldrich, Israel), and the temperature was reduced to 28 °C for overnight incubation. Periplasmic extracts, containing the soluble proteins (N-TIMP2 and N-TIMP2-S31PrK), were obtained by osmotic shock using 9 mL of TES buffer (500 mM sucrose, 200 mM Tris-HCl, 0.5 mM EDTA, pH 8) per cell pellet [generated from 500 mL of culture (with a final OD<sub>600</sub> < 20)], for 3 h at 4 °C and 200 rpm, followed by adding 18 mL of TES buffer (diluted 1:4 in doubly distilled water) for overnight incubation. The proteins were purified using affinity chromatography on Ni-NTA gravitational beads (Invitrogen, CA) and eluted with 0.5 M imidazole in phosphate-buffered saline (PBS). The eluted fraction was dialyzed against PBS, and the size and purity of the proteins were evaluated using SDS-PAGE gel electrophoresis and mass spectrometry (MALDI-TOF Reflex-IV, Ilse Katz Institute for Nanoscale Science and Technology, BGU, Israel). For LC-MS/MS analysis of N-TIMP2-S31PrK, excised SDS-PAGE gel bands

were denatured, reduced, alkylated, and digested with trypsin. The digested peptides were then subjected to tandem mass spectrometry analysis by the LTQ-Orbitrap XL ETD system (Ilse Katz Institute for Nanoscale Science and Technology Shared Resource Facility, BGU, Israel). Protein concentrations were determined by UV-vis absorbance at 280 nm, using a NanoDrop spectrophotometer (Thermo Fisher Scientific), with an extinction coefficient ( $\epsilon_{280}$ ) of 13,500  $M^{-1} \text{ cm}^{-1}$  for all N-TIMP2 variants.

Small-scale expression of N-TIMP2-S31PrK (used only for analysis) was performed in 10 mL of TB medium overnight, as described above, in the presence or absence of PrK, IPTG, and arabinose. Protein expression was determined by western blotting, using a 1:3000 dilution of mouse anti-6XHis primary antibody (ab49936, monoclonal, HIS-1, Abcam, Cambridge, U.K.), followed by a 1:2000 dilution of anti-mouse secondary antibody conjugated to horseradish peroxidase (HRP) (CST-7076S, Cell Signaling Tech) and detection by chemiluminescent reagents (EZ-ECL, BI, Israel).

**MMP-14 Inhibition Studies.** The inhibition constant ( $K_i$ ) of N-TIMP2 proteins against the catalytic domain of MMP-14 (MMP-14<sub>CAT</sub>) was determined as previously described.<sup>55</sup> The inhibition of the catalytic activity of MMP-14<sub>CAT</sub> (0.0075 nM) measured against the fluorogenic substrate Mca-Pro-Leu-Gly-Leu-Dpa-Ala-Arg-NH<sub>2</sub>-TFA (7.5  $\mu\text{M}$ , Merck Millipore) was determined with N-TIMP2<sub>D</sub>, N-TIMP2<sub>D-Cys</sub>, and N-TIMP2<sub>D-Cys-PEG</sub> at 0–0.18 nM or with N-TIMP2, N-TIMP2-S31PrK, and N-TIMP2-PEG20K at 0–3 nM.  $K_i$  was calculated according to Morrison's equation (eq 1), the classic competitive inhibition equation for tight binding, using Prism (GraphPad Software). Mean values of  $K_i \pm$  standard error of the mean (SEM) were obtained from three independent experiments.

$$\frac{V_i}{V_0} = 1 - \frac{([E] + [I] + K_i^{\text{app}}) - \sqrt{([E] + [I] + K_i^{\text{app}})^2 - 4[E][I]}}{2[E]} \quad (1)$$

where  $V_i$  is the enzyme velocity in the presence of an inhibitor,  $V_0$  is the enzyme velocity in the absence of an inhibitor,  $E$  is the enzyme concentration,  $I$  is the inhibitor concentration,  $S$  is the substrate concentration,  $K_M$  is the Michaelis–Menten constant, and  $K_i^{\text{app}}$  is the apparent inhibition constant, which is given by eq 2

$$K_i^{\text{app}} = K_i \left( 1 + \frac{[S]}{K_m} \right) \quad (2)$$

where  $K_i$  is the inhibition constant.

Statistical analysis was performed using Student's *t*-test.

**Fluorescent Labeling by a Click Chemistry Reaction.** N-TIMP2 and N-TIMP2-S31PrK were labeled using a Cu(I)-catalyzed azide–alkyne cycloaddition reaction (CuAAC), as previously described with some modifications.<sup>71</sup> Briefly, the N-TIMP2 protein was added to a reaction solution containing 100 mM NaH<sub>2</sub>PO<sub>4</sub> pH 7.0, 0.2 mM CuSO<sub>4</sub>, 1.2 mM 3,3',3''-(4,4',4''-(nitrioltris(methylene))tris(1H-1,2,3-triazole-4,1-diyl))tris(propan-1-ol) (THPTA; Sigma-Aldrich, Israel), and 0.05 mM of either tetramethylrhodamine-azide (TAMRA-AZ; Sigma-Aldrich) or Cyanine5.5 azide (Cy5.5-Az; Lumiprobe, MD). Sodium ascorbate was added to a final concentration of 2.5 mM, and the reaction mixture (50  $\mu\text{L}$ ) was incubated at room temperature for 1 h. SDS-PAGE analysis on an 18% polyacrylamide gel was then performed under reducing

conditions. Labeled proteins were visualized in-gel using a Typhoon FLA 9500 imager (GE Healthcare Life Sciences, Uppsala, Sweden), set in the TAMRA fluorescence mode (excitation: 542 nm; emission: 525 nm) for TAMRA-Az or the Cy5 fluorescence mode (excitation: 649 nm; emission: 670 nm) for Cy5.5-Az.

**PEGylation of N-TIMP2-S31PrK.** N-TIMP2-S31PrK was PEGylated with methoxy PEG azide having a molecular weight of 20 kDa (mPEG-azide-20K) (Jenkem, TX) by click chemistry. For the small-scale PEGylation reaction, CuSO<sub>4</sub> (0.5 mM) and THPTA (2.5 mM) were premixed for 20 min. Thereafter, N-TIMP2-S31PrK (0.04 mM), mPEG-azide-20K (to reach a 1:100–1:600 protein:PEG molar ratio), and 100 mM phosphate buffer, pH 7.0 (to reach the final reaction volume of 50  $\mu$ L) were added, followed by sodium ascorbate (5 mM). The tube containing the reaction mixture was then sealed and gently rocked at 37 °C for 2 h. The reaction mixture was analyzed by SDS-PAGE using 15% polyacrylamide under reducing conditions, and the conversion yields were quantified by ImageJ. For the large-scale PEGylation reaction, the same method as that described above was used with 1 mg of N-TIMP2-S31PrK and a 1:400 protein:PEG molar ratio. The PEGylated protein was purified as follows: the reaction solution was dialyzed against buffer A (50 mM NaH<sub>2</sub>PO<sub>4</sub>–NaOH, pH 6.0) for 48 h to remove the Cu ions and then loaded onto a Resource S cation-exchange column (GE Healthcare, MA). Buffer A was used for washing, and a linear gradient of 0–50% of buffer B (50 mM NaH<sub>2</sub>PO<sub>4</sub>–NaOH, pH 6.0, 0.5 M NaCl) was used for elution. The sample was then dialyzed against PBS (pH 7.4) and analyzed by SDS-PAGE using 15% polyacrylamide under reducing conditions and staining for protein and PEG visualization. Briefly, the gel was washed twice with doubly distilled water, incubated with freshly made 5% BaCl<sub>2</sub> (Sigma-Aldrich, Israel) for 10 min, and then developed with 2% iodine solution (Hylabs, Israel). After PEG visualization, the gel was washed with doubly distilled water and stained with Coomassie blue for protein visualization.

**Serum Stability Assay.** N-TIMP2 or N-TIMP2-PEG20K (at 0.7 mg/mL) was diluted (1:5 v/v) in human serum (from a healthy volunteer). The tubes were sealed and incubated at 37 °C for a period of 18 days. Aliquots were withdrawn from each tube every 2–4 days and stored at –80 °C until analysis. Each sample (1  $\mu$ L) was subjected to an anti-6 $\times$ His western blot analysis, as described above, and protein levels were quantified using ImageJ. Statistical significance was determined by Student's *t*-test; *p* < 0.05 was considered significant.

**Pharmacokinetic Studies.** BALB/c female mice (6 weeks old) were injected intravenously with 200  $\mu$ L of 3 mg/kg N-TIMP2 or N-TIMP2-PEG20K proteins, and serial blood samples were drawn from the tail vein over 8 h for N-TIMP2 and over 72 h for N-TIMP2-PEG20K, with three mice for each time point. Serum was separated from the blood using Minicollect (Greiner, Germany), according to the manufacturer's protocol.

Serum protein concentrations were determined using a sandwich enzyme-linked immunosorbent assay (ELISA) in a high binding 96-well Nunc MaxiSorp plate (Thermo Fisher Scientific). The plate was coated with 100  $\mu$ L of 2  $\mu$ g/mL anti-TIMP2 antibody (ab180630, polyclonal, Abcam, U.K.) in PBS overnight at 4 °C. The solution containing anti-N-TIMP2 antibody was discarded, and the wells were washed three times with PBST (PBS with 0.05% Tween-20) and blocked with 5%

bovine serum albumin (Chem-Impex, IL) for 2 h at room temperature. The blocking solution was then discarded, the wells were washed three times with PBST, and the serum samples containing N-TIMP2 or N-TIMP2-PEG20K were added (in duplicate for each sample) and incubated overnight at 4 °C. A standard curve was generated by making serial dilutions of N-TIMP2 or N-TIMP2-PEG20K dissolved in mouse serum (Sigma-Aldrich, MO). Wells were washed three times with PBST and a detection antibody, 100  $\mu$ L of 0.25  $\mu$ g/mL anti-6 $\times$ His tag HRP conjugated (ab1187, polyclonal, Abcam, U.K.), was added and incubated overnight at 4 °C. Wells were then washed three times with PBST, and an HRP substrate, namely, TMB (3,3',5,5'-tetramethylbenzidine) (Dako, Glostrup, Denmark), was added and incubated until the color was observed. A stop solution, 1 M H<sub>2</sub>SO<sub>4</sub>, was then added, and the chromogenic reactions were measured using a plate reader (Biotek, VT) at 450 nm. A graph of serum concentration vs time was plotted, and the noncompartmental pharmacokinetic analysis of the data [to calculate values for the half-life (*t*<sub>1/2</sub>) and area under the curve (AUC<sub>0–∞</sub>)] was performed using the PKSolver 2.0 Microsoft Excel add-in.<sup>72</sup>

## ■ ASSOCIATED CONTENT

### Supporting Information

The Supporting Information is available free of charge at <https://pubs.acs.org/doi/10.1021/acs.bioconjchem.2c00059>.

PrK and the protein structure; supplementary western blot analysis; and supplementary SDS-PAGE (PDF)

## ■ AUTHOR INFORMATION

### Corresponding Author

**Niv Papo** – Avram and Stella Goldstein-Goren Department of Biotechnology Engineering, Ben-Gurion University of the Negev, Beer-Sheva 84105, Israel; The National Institute of Biotechnology in the Negev, Ben-Gurion University of the Negev, Beer-Sheva 84105, Israel; [orcid.org/0000-0002-7056-2418](https://orcid.org/0000-0002-7056-2418); Phone: +972-50-2029729; Email: [papo@bgu.ac.il](mailto:papo@bgu.ac.il)

### Authors

**Hezi Hayun** – Avram and Stella Goldstein-Goren Department of Biotechnology Engineering, Ben-Gurion University of the Negev, Beer-Sheva 84105, Israel; The National Institute of Biotechnology in the Negev, Ben-Gurion University of the Negev, Beer-Sheva 84105, Israel

**Valeria Arkadash** – Avram and Stella Goldstein-Goren Department of Biotechnology Engineering, Ben-Gurion University of the Negev, Beer-Sheva 84105, Israel; The National Institute of Biotechnology in the Negev, Ben-Gurion University of the Negev, Beer-Sheva 84105, Israel

**Amiram Sananes** – Avram and Stella Goldstein-Goren Department of Biotechnology Engineering, Ben-Gurion University of the Negev, Beer-Sheva 84105, Israel; The National Institute of Biotechnology in the Negev, Ben-Gurion University of the Negev, Beer-Sheva 84105, Israel

**Eyal Arbely** – Department of Chemistry and The National Institute of Biotechnology in the Negev, Ben-Gurion University of the Negev, Beer-Sheva 84105, Israel; [orcid.org/0000-0002-0284-0092](https://orcid.org/0000-0002-0284-0092)

**David Stepensky** – Department of Clinical Biochemistry and Pharmacology, Faculty of Health Sciences, Ben-Gurion University of the Negev, Beer-Sheva 8410501, Israel

Complete contact information is available at:  
<https://pubs.acs.org/10.1021/acs.bioconjchem.2c00059>

## Notes

The authors declare no competing financial interest.

## ACKNOWLEDGMENTS

The authors thank Dr. Mark Karpasas for his professional assistance with the MS experiments. MS experiments were performed at the Ilse Katz Institute for Nanoscale Science and Technology, BGU.

## ABBREVIATIONS

BGU, Ben-Gurion University of the Negev; ECM, extracellular matrix; MMP, matrix metalloproteinase; NCAA, noncanonical amino acid; PEG, poly(ethylene glycol); PrK, propargyl lysine; TIMP, tissue inhibitor of matrix metalloproteinase

## REFERENCES

- (1) Visse, R.; Nagase, H. Matrix metalloproteinases and tissue inhibitors of metalloproteinases: structure, function, and biochemistry. *Circ. Res.* **2003**, *92*, 827–839.
- (2) Lu, H.; Cao, X.; Zhang, H.; Sun, G.; Fan, G.; Chen, L.; Wang, S. Imbalance between MMP-2, 9 and TIMP-1 promote the invasion and metastasis of renal cell carcinoma via SKP2 signaling pathways. *Tumor Biol.* **2014**, *35*, 9807–9813.
- (3) Murphy, G.; Nagase, H. Progress in matrix metalloproteinase research. *Mol. Aspects Med.* **2008**, *29*, 290–308.
- (4) Egeblad, M.; Werb, Z. New functions for the matrix metalloproteinases in cancer progression. *Nat. Rev. Cancer* **2002**, *2*, 161–174.
- (5) Kenny, H. A.; Kaur, S.; Coussens, L. M.; Lengyel, E. The initial steps of ovarian cancer cell metastasis are mediated by MMP-2 cleavage of vitronectin and fibronectin. *J. Clin. Invest.* **2008**, *118*, 1367–1379.
- (6) Morgia, G.; Falsaperla, M.; Malaponte, G.; Madonia, M.; Indelicato, M.; Travali, S.; Mazzarino, M. C. Matrix metalloproteinases as diagnostic (MMP-13) and prognostic (MMP-2, MMP-9) markers of prostate cancer. *Urol. Res.* **2005**, *33*, 44–50.
- (7) Coussens, L. M.; Fingleton, B.; Matrisian, L. M. Matrix metalloproteinase inhibitors and cancer: trials and tribulations. *Science* **2002**, *295*, 2387–2392.
- (8) Michael, M.; Babic, B.; Khokha, R.; Tsao, M.; Ho, J.; Pintilie, M.; Leco, K.; Chamberlain, D.; Shepherd, F. A. Expression and prognostic significance of metalloproteinases and their tissue inhibitors in patients with small-cell lung cancer. *J. Clin. Oncol.* **1999**, *17*, 1802–1808.
- (9) Têtu, B.; Brisson, J.; Wang, C. S.; Lapointe, H.; Beaudry, G.; Blanchette, C.; Trudel, D. The influence of MMP-14, TIMP-2 and MMP-2 expression on breast cancer prognosis. *Breast Cancer Res.* **2006**, *8*, No. R28.
- (10) Yang, B.; Gao, J.; Rao, Z.; Shen, Q. Clinicopathological and prognostic significance of alpha5beta1-integrin and MMP-14 expressions in colorectal cancer. *Neoplasma* **2013**, *60*, 254–261.
- (11) Harada, T.; Arai, S.; Mise, M.; Imamura, T.; Higashitsuji, H.; Furutani, M.; Niwano, M.; Ishigami, S.; Fukumoto, M.; Seiki, et al. Membrane-type matrix metalloproteinase-1 (MT1-MMP) gene is overexpressed in highly invasive hepatocellular carcinomas. *J. Hepatol.* **1998**, *28*, 231–239.
- (12) Zhang, H.; Liu, M.; Sun, Y.; Lu, J. MMP-14 can serve as a prognostic marker in patients with supraglottic cancer. *Eur. Arch. Oto-Rhino-Laryngol.* **2009**, *266*, 1427–1434.
- (13) Kerkelä, E.; Ala-aho, R.; Lohi, J.; Grenman, R.; V, M. K.; Saarialho-Kere, U. Differential patterns of stromelysin-2 (MMP-10) and MT1-MMP (MMP-14) expression in epithelial skin cancers. *Br. J. Cancer* **2001**, *84*, 659–669.
- (14) Bartolomé, R. A.; Ferreiro, S.; Miquilena-Colina, M. E.; Martínez-Prats, L.; Soto-Montenegro, M. L.; García-Bernal, D.; Vaquero, J. J.; Agami, R.; Delgado, R.; Desco, M.; et al. The chemokine receptor CXCR4 and the metalloproteinase MT1-MMP are mutually required during melanoma metastasis to lungs. *Am. J. Pathol.* **2009**, *174*, 602–612.
- (15) Adley, B. P.; Gleason, K. J.; Yang, X. J.; Stack, M. S. Expression of membrane type 1 matrix metalloproteinase (MMP-14) in epithelial ovarian cancer: high level expression in clear cell carcinoma. *Gynecol. Oncol.* **2009**, *112*, 319–324.
- (16) Schmalfeldt, B.; Prechtel, D.; Harting, K.; Spathe, K.; Rutke, S.; Konik, E.; Fridman, R.; Berger, U.; Schmitt, M.; Kuhn, W.; et al. Increased expression of matrix metalloproteinases (MMP)-2, MMP-9, and the urokinase-type plasminogen activator is associated with progression from benign to advanced ovarian cancer. *Clin. Cancer Res.* **2001**, *7*, 2396–2404.
- (17) Stetler-Stevenson, W. G. Matrix metalloproteinases in angiogenesis: a moving target for therapeutic intervention. *J. Clin. Invest.* **1999**, *103*, 1237–1241.
- (18) Sato, H.; Takino, T. Coordinate action of membrane-type matrix metalloproteinase-1 (MT1-MMP) and MMP-2 enhances pericellular proteolysis and invasion. *Cancer Sci.* **2010**, *101*, 843–847.
- (19) Overall, C. M.; Kleinfeld, O. Tumour microenvironment-opinion: validating matrix metalloproteinases as drug targets and anti-targets for cancer therapy. *Nat. Rev. Cancer* **2006**, *6*, 227–239.
- (20) López-Otín, C.; Matrisian, L. M. Emerging roles of proteases in tumour suppression. *Nat. Rev. Cancer* **2007**, *7*, 800–808.
- (21) Yue, L.; Shi, Y.; Su, X.; Ouyang, L.; Wang, G.; Ye, T. Matrix metalloproteinases inhibitors in idiopathic pulmonary fibrosis: Medicinal chemistry perspectives. *Eur. J. Med. Chem.* **2021**, *224*, No. 113714.
- (22) Sela-Passwell, N.; Kikkeri, R.; Dym, O.; Rozenberg, H.; Margalit, R.; Arad-Yellin, R.; Eisenstein, M.; Brenner, O.; Shoham, T.; Danon, T.; Shanzer, A.; et al. Antibodies targeting the catalytic zinc complex of activated matrix metalloproteinases show therapeutic potential. *Nat. Med.* **2012**, *18*, 143–147.
- (23) Devy, L.; Huang, L.; Naa, L.; Yanamandra, N.; Pieters, H.; Frans, N.; Chang, E.; Tao, Q.; Vanhove, M.; Lejeune, et al. Selective inhibition of matrix metalloproteinase-14 blocks tumor growth, invasion, and angiogenesis. *Cancer Res.* **2009**, *69*, 1517–1526.
- (24) Roque, A. C.; Lowe, C. R.; Taipa, M. A. Antibodies and genetically engineered related molecules: production and purification. *Biotechnol. Prog.* **2004**, *20*, 639–654.
- (25) Romer, T.; Leonhardt, H.; Rothbauer, U. Engineering antibodies and proteins for molecular in vivo imaging. *Curr. Opin. Biotechnol.* **2011**, *22*, 882–887.
- (26) McCamish, M.; Woollett, G. Worldwide experience with biosimilar development. *mAbs* **2011**, *3*, 209–217.
- (27) Nagase, H.; Visse, R.; Murphy, G. Structure and function of matrix metalloproteinases and TIMPs. *Cardiovasc. Res.* **2006**, *69*, 562–573.
- (28) Murphy, G. Tissue inhibitors of metalloproteinases. *Genome Biol.* **2011**, *12*, No. 233.
- (29) Hernandez-Barrantes, S.; Toth, M.; Bernardo, M. M.; Yurkova, M.; Gervasi, D. C.; Raz, Y.; Sang, Q. A.; Fridman, R. Binding of active (57 kDa) membrane type 1-matrix metalloproteinase (MT1-MMP) to tissue inhibitor of metalloproteinase (TIMP)-2 regulates MT1-MMP processing and pro-MMP-2 activation. *J. Biol. Chem.* **2000**, *275*, 12080–12089.
- (30) Itoh, Y.; Seiki, M. MT1-MMP: an enzyme with multidimensional regulation. *Trends Biochem. Sci.* **2004**, *29*, 285–289.
- (31) Mohan, V.; Talmi-Frank, D.; Arkadash, V.; Papo, N.; Sagi, I. Matrix metalloproteinase protein inhibitors: highlighting a new beginning for metalloproteinases in medicine. *Metalloproteinases Med.* **2016**, *3*, 31–47.
- (32) Morgunova, E.; Tuuttila, A.; Bergmann, U.; Tryggvason, K. Structural insight into the complex formation of latent matrix metalloproteinase 2 with tissue inhibitor of metalloproteinase 2. *Proc. Natl. Acad. Sci. U.S.A.* **2002**, *99*, 7414–7419.

- (33) Butler, G. S.; Hutton, M.; Wattam, B. A.; Williamson, R. A.; Knauper, V.; Willenbrock, F.; Murphy, G. The specificity of TIMP-2 for matrix metalloproteinases can be modified by single amino acid mutations. *J. Biol. Chem.* **1999**, *274*, 20391–20396.
- (34) Kurschat, P.; Graeve, L.; Erren, A.; Gatsios, P.; Rose-John, S.; Roeb, E.; Tschesche, H.; Koj, A.; Heinrich, P. C. Expression of a biologically active murine tissue inhibitor of metalloproteinases-1 (TIMP-1) in baculovirus-infected insect cells. Purification and tissue distribution in the rat. *Eur. J. Biochem.* **1995**, *234*, 485–491.
- (35) Black, R. A.; Durie, F. H.; Otten-Evans, C.; Miller, R.; Slack, J. L.; Lynch, D. H.; Castner, B.; Mohler, K. M.; Gerhart, M.; Johnson, R. S.; et al. Relaxed specificity of matrix metalloproteinases (MMPS) and TIMP insensitivity of tumor necrosis factor-alpha (TNF-alpha) production suggest the major TNF-alpha converting enzyme is not an MMP. *Biochem. Biophys. Res. Commun.* **1996**, *225*, 400–405.
- (36) Batra, J.; Robinson, J.; Mehner, C.; Hockla, A.; Miller, E.; Radisky, D. C.; Radisky, E. S. PEGylation extends circulation half-life while preserving in vitro and in vivo activity of tissue inhibitor of metalloproteinases-1 (TIMP-1). *PLoS One* **2012**, *7*, No. e50028.
- (37) Kulasegaram, R.; Giersing, B.; Page, C. J.; Blower, P. J.; Williamson, R. A.; Peters, B. S.; O'Doherty, M. J. In vivo evaluation of <sup>111</sup>In-DTPA-N-TIMP-2 in Kaposi sarcoma associated with HIV infection. *Eur. J. Nucl. Med.* **2001**, *28*, 756–761.
- (38) Deiters, A.; Cropp, T. A.; Summerer, D.; Mukherji, M.; Schultz, P. G. Site-specific PEGylation of proteins containing unnatural amino acids. *Bioorg. Med. Chem. Lett.* **2004**, *14*, 5743–5745.
- (39) Delgado, C.; Pedley, R. B.; Herraes, A.; Boden, R.; Boden, J. A.; Keep, P. A.; Chester, K. A.; Fisher, D.; Begent, R. H.; Francis, G. E. Enhanced tumour specificity of an anti-carcinoembryonic antigen Fab' fragment by poly(ethylene glycol) (PEG) modification. *Br. J. Cancer* **1996**, *73*, 175–182.
- (40) Chapman, A. P.; Antoniow, P.; Spitali, M.; West, S.; Stephens, S.; King, D. J. Therapeutic antibody fragments with prolonged in vivo half-lives. *Nat. Biotechnol.* **1999**, *17*, 780–783.
- (41) Lieser, R. M.; Yur, D.; Sullivan, M. O.; Chen, W. Site-Specific Bioconjugation Approaches for Enhanced Delivery of Protein Therapeutics and Protein Drug Carriers. *Bioconjugate Chem.* **2020**, *31*, 2272–2282.
- (42) Wu, L.; Chen, J.; Wu, Y.; Zhang, B.; Cai, X.; Zhang, Z.; Wang, Y.; Si, L.; Xu, H.; Zheng, Y.; et al. Precise and combinatorial PEGylation generates a low-immunogenic and stable form of human growth hormone. *J. Controlled Release* **2017**, *249*, 84–93.
- (43) Nairn, N. W.; Shanebeck, K. D.; Wang, A.; Graddis, T. J.; VanBrunt, M. P.; Thornton, K. C.; Grabstein, K. Development of copper-catalyzed azide-alkyne cycloaddition for increased in vivo efficacy of interferon beta-1b by site-specific PEGylation. *Bioconjugate Chem.* **2012**, *23*, 2087–2097.
- (44) Simon, M.; Stefan, N.; Borsig, L.; Pluckthun, A.; Zangemeister-Wittke, U. Increasing the antitumor effect of an EpCAM-targeting fusion toxin by facile click PEGylation. *Mol. Cancer Ther.* **2014**, *13*, 375–385.
- (45) Wan, W.; Tharp, J. M.; Liu, W. R. Pyrrolysyl-tRNA synthetase: an ordinary enzyme but an outstanding genetic code expansion tool. *Biochim. Biophys. Acta, Proteins Proteomics* **2014**, *1844*, 1059–1070.
- (46) Chin, J. W. Expanding and reprogramming the genetic code. *Nature* **2017**, *550*, 53–60.
- (47) Zimmerman, E. S.; Heibeck, T. H.; Gill, A.; Li, X.; Murray, C. J.; Madlansacay, M. R.; Tran, C.; Uter, N. T.; Yin, G.; Rivers, P. J.; et al. Production of site-specific antibody-drug conjugates using optimized non-natural amino acids in a cell-free expression system. *Bioconjugate Chem.* **2014**, *25*, 351–361.
- (48) Aloush, N.; Schwartz, T.; Konig, A. I.; Cohen, S.; Brozgol, E.; Tam, B.; Nachmias, D.; Ben-David, O.; Garini, Y.; Elia, N.; et al. Live Cell Imaging of Bioorthogonally Labelled Proteins Generated With a Single Pyrrolysine tRNA Gene. *Sci. Rep.* **2018**, *8*, No. 14527.
- (49) Lang, K.; Chin, J. W. Cellular incorporation of unnatural amino acids and bioorthogonal labeling of proteins. *Chem. Rev.* **2014**, *114*, 4764–4806.
- (50) Tamshen, K.; Wang, Y.; Jamieson, S. M. F.; Perry, J. K.; Maynard, H. D. Genetic Code Expansion Enables Site-Specific PEGylation of a Human Growth Hormone Receptor Antagonist through Click Chemistry. *Bioconjugate Chem.* **2020**, *31*, 2179–2190.
- (51) Hutchins, B. M.; Kazane, S. A.; Staffin, K.; Forsyth, J. S.; Felding-Habermann, B.; Schultz, P. G.; Smider, V. V. Site-specific coupling and sterically controlled formation of multimeric antibody Fab fragments with unnatural amino acids. *J. Mol. Biol.* **2011**, *406*, 595–603.
- (52) Zhang, J.; Yan, S.; He, Z.; Ding, C.; Zhai, T.; Chen, Y.; Li, H.; Yang, G.; Zhou, X.; Wang, P. Small Unnatural Amino Acid Carried Raman Tag for Molecular Imaging of Genetically Targeted Proteins. *J. Phys. Chem. Lett.* **2018**, *9*, 4679–4685.
- (53) Wissler, H. L.; Ehlerding, E. B.; Lyu, Z.; Zhao, Y.; Zhang, S.; Eshraghi, A.; Buuh, Z. Y.; McGuth, J. C.; Guan, Y.; Engle, J. W.; et al. Site-Specific Immuno-PET Tracer to Image PD-L1. *Mol. Pharmacol.* **2019**, *16*, 2028–2036.
- (54) Sharabi, O.; Shirian, J.; Grossman, M.; Lebendiker, M.; Sagi, I.; Shifman, J. Affinity- and specificity-enhancing mutations are frequent in multispecific interactions between TIMP2 and MMPs. *PLoS One* **2014**, *9*, No. e93712.
- (55) Arkadash, V.; Yosef, G.; Shirian, J.; Cohen, I.; Horev, Y.; Grossman, M.; Sagi, I.; Radisky, E. S.; Shifman, J. M.; Papo, N. Development of High Affinity and High Specificity Inhibitors of Matrix Metalloproteinase 14 through Computational Design and Directed Evolution. *J. Biol. Chem.* **2017**, *292*, 3481–3495.
- (56) Veronese, F. M.; Mero, A. The impact of PEGylation on biological therapies. *BioDrugs* **2008**, *22*, 315–329.
- (57) Wang, J. H.; Tam, S. C.; Huang, H.; Ouyang, D. Y.; Wang, Y. Y.; Zheng, Y. T. Site-directed PEGylation of trichostanthin retained its anti-HIV activity with reduced potency in vitro. *Biochem. Biophys. Res. Commun.* **2004**, *317*, 965–971.
- (58) Fernandez-Catalan, C.; Bode, W.; Huber, R.; Turk, D.; Calvete, J. J.; Lichte, A.; Tschesche, H.; Maskos, K. Crystal structure of the complex formed by the membrane type 1-matrix metalloproteinase with the tissue inhibitor of metalloproteinases-2, the soluble progelatinase A receptor. *EMBO J.* **1998**, *17*, 5238–5248.
- (59) Young, T. S.; Ahmad, I.; Yin, J. A.; Schultz, P. G. An enhanced system for unnatural amino acid mutagenesis in *E. coli*. *J. Mol. Biol.* **2010**, *395*, 361–374.
- (60) Zhang, Y.; Ptacin, J. L.; Fischer, E. C.; Aerni, H. R.; Caffaro, C. E.; San Jose, K.; Feldman, A. W.; Turner, C. R.; Romesberg, F. E. A semi-synthetic organism that stores and retrieves increased genetic information. *Nature* **2017**, *551*, 644–647.
- (61) Cohen, M.; Ozer, E.; Kushmaro, A.; Alfonta, L. Cellular localization of cytochrome bd in cyanobacteria using genetic code expansion. *Biotechnol. Bioeng.* **2020**, *117*, 523–530.
- (62) Yosef, G.; Arkadash, V.; Papo, N. Targeting the MMP-14/MMP-2/integrin alpha<sub>v</sub>beta<sub>3</sub> axis with multispecific N-TIMP2-based antagonists for cancer therapy. *J. Biol. Chem.* **2018**, *293*, 13310–13326.
- (63) Zheng, C.; Ma, G.; Su, Z. Native PAGE eliminates the problem of PEG-SDS interaction in SDS-PAGE and provides an alternative to HPLC in characterization of protein PEGylation. *Electrophoresis* **2007**, *28*, 2801–2807.
- (64) Veronese, F. M.; Caliceti, P.; Schiavon, O. Branched and Linear Poly(Ethylene Glycol): Influence of the Polymer Structure on Enzymological, Pharmacokinetic, and Immunological Properties of Protein Conjugates. *J. Bioact. Compat. Polym.* **1997**, *12*, 196–207.
- (65) Lawrence, P. B.; Gavrilov, Y.; Matthews, S. S.; Langlois, M. I.; Shental-Bechor, D.; Greenblatt, H. M.; Pandey, B. K.; Smith, M. S.; Paxman, R.; Torgerson, C. D.; et al. Criteria for selecting PEGylation sites on proteins for higher thermodynamic and proteolytic stability. *J. Am. Chem. Soc.* **2014**, *136*, 17547–17560.
- (66) Lawrence, P. B.; Price, J. L. How PEGylation influences protein conformational stability. *Curr. Opin. Chem. Biol.* **2016**, *34*, 88–94.
- (67) Harris, J. M.; Chess, R. B. Effect of pegylation on pharmaceuticals. *Nat. Rev. Drug Discovery* **2003**, *2*, 214–221.

(68) Tsutsumi, Y.; Tsunoda, S.; Kamada, H.; Kihira, T.; Kaneda, Y.; Ohsugi, Y.; Mayumi, T. PEGylation of interleukin-6 effectively increases its thrombopoietic potency. *Thromb. Haemostasis* **1997**, *77*, 168–173.

(69) Tsutsumi, Y.; Kihira, T.; Tsunoda, S.; Kanamori, T.; Nakagawa, S.; Mayumi, T. Molecular design of hybrid tumour necrosis factor alpha with polyethylene glycol increases its anti-tumour potency. *Br. J. Cancer* **1995**, *71*, 963–968.

(70) Peleg, Y.; Unger, T. Application of the Restriction-Free (RF) cloning for multicomponents assembly. *Methods Mol. Biol.* **2014**, *1116*, 73–87.

(71) Ozer, E.; Chemla, Y.; Schlesinger, O.; Aviram, H. Y.; Riven, L.; Haran, G.; Alfonta, L. In vitro suppression of two different stop codons. *Biotechnol. Bioeng.* **2017**, *114*, 1065–1073.

(72) Zhang, Y.; Huo, M.; Zhou, J.; Xie, S. PKSolver: An add-in program for pharmacokinetic and pharmacodynamic data analysis in Microsoft Excel. *Comput. Methods Programs Biomed.* **2010**, *99*, 306–314.